[American Journal of Science, Vol. 304, June, 2004, P. 533–557]

METAL TRANSPORT AND DEPOSITION IN HYDROTHERMAL VEINS REVEALED BY 213nm UV LASER ABLATION MICROANALYSIS OF SINGLE FLUID INCLUSIONS

B. STOFFELL*, J. J. WILKINSON* and T. E. JEFFRIES**

ABSTRACT. 213nm UV laser ablation provides a powerful and cost-effective new method for the chemical microanalysis of individual fluid inclusions. The instrument offers significantly improved energy absorption in many geological materials compared to 266nm UV lasers resulting in improved ablation characteristics. The laser is not strongly absorbed by either air or commonly used optical material, permitting relatively easy delivery and control of the beam.

Ablation of multielement standard solutions in pure quartz glass capillaries was found to be an effective method for external calibration of instrument sensitivity. Internal calibration for calculation of absolute element concentrations in inclusion fluids was carried out using chloride concentration estimated from microthermometric data. Using this approach, analyses of groups of cogenetic primary and secondary inclusions using a 30 element analyte menu gave typical relative standard deviations for absolute element concentrations of around 20 percent for alkali and alkali earth elements and 20 to 50 percent for metals, comparable with those obtained by 193nm Excimer laser ablation. Results for Ca are consistent with independent estimates made from microthermometric measurements and a range of other elements are in reasonable agreement with previously published bulk chemical analyses. Overall, the data give good charge balance, within 5 percent.

The technique was used to test the hypothesis that the metal content of hydrothermal ore deposits is primarily controlled by the metal content of the mineralizing solutions rather than selective precipitation mechanisms. We studied Pb(-Zn) mineralized 'crosscourse' veins from Southwest England that are known to have formed from low temperature brines expelled from Permo-Triassic red-bed basins adjacent to the Cornubian peninsula, probably during the Triassic. These fluids are comparable with the solutions that formed Mississippi Valley-type Pb-Zn deposits.

Analyses of primary fluid inclusions across growth-zoned quartz crystals from one of these veins indicate the orefluids at an early stage of vein growth are relatively Pb-rich (up to 295 ppm Pb, up to 86 ppm Zn; Pb/Zn = 1.3-16.1) and display marked temporal variations in chemistry. Gradual increases in K, Ca, Sr, Ba and Zn are observed across a significant (~10 mm) interval of quartz growth. These increases are interpreted to reflect mineral dissolution-precipitation reactions occurring within the fracture system exploited by the fluids after being expelled from the basin source area. Superimposed on this trend are comparatively short time-scale (~1 mm of quartz growth) chemical excursions characterized by decreases in the concentrations of Cl, K, Ca, Ba, Sr, Pb and Zn of up to two orders of magnitude. These excursions are believed to be due to local, volumetrically significant, mineral precipitation events and indicate the operation of processes that result in the simultaneous supersaturation of a number of phases.

It is suggested that initial galena precipitation (>98% Pb loss from solution) was due to reduction as oxidized fluids encountered the first strongly reducing lithology on their flow path out of the basin source region. Several later dilution events were caused by fluid mixing and are inferred to have caused the co-precipitation of sulfides (galena, sphalerite; up to 98% loss of metals from solution) with sulfates (anhydrite, barite; up to 91% Ca and 97% Ba loss from solution) and/or silicates (K-mica; up to 96% loss of K from solution). However, at only one stage is galena (±anhydrite, K-mica) observed in

*Department of Earth Science and Engineering, Imperial College London, South Kensington Campus, Exhibition Road, London SW7 2AZ, United Kingdom; barry.stoffell@imperial.ac.uk; j.wilkinson@imperial.ac.uk

**Department of Mineralogy, The Natural History Museum, Cromwell Road, London SW7 5BD, United Kingdom

the sample studied suggesting that fluid inclusions may commonly trap depleted fluids after mineral precipitation has already occurred some distance upstream, rather than reflecting precipitation events in their immediate vicinity.

The primary ore-forming fluid in this case study contained elevated Pb and Zn and, at least initially, displayed a higher Pb/Zn ratio than predicted for fluids saturated with respect to both sphalerite and galena. Therefore, we suggest that the Pb-rich tenor of the vein deposit is primarily controlled by the metal content of the ore fluids, which is ultimately a function of the geochemistry of the basin source. In this example, the source area is dominated by oxidized terrestrial clastic rocks. Reactions within the aquifer and selective precipitation mechanisms at the site of ore formation also appear to have modified fluid geochemistry but played a second order role in controlling the metal budget of the mineral deposit formed.

INTRODUCTION

Low-temperature (<150°C), high-salinity (>20 wt% dissolved salts) aqueous fluids are often involved in the transport and deposition of metals within the crust, yet our knowledge of the chemistry of such brines, in particular their metal content, is incomplete. The mineralizing fluids responsible for the formation of Mississippi Valley-Type deposits, a major global source of Pb and Zn, are a good example. Despite extensive research, the controls of metal ratios in these deposits, the metal content of ore fluids and the mechanisms of metal transport and deposition are often poorly constrained (Skinner, 1997). Much of this uncertainty stems from the difficulties inherent in the analysis of the chemistry of the microscopic fluid inclusions that provide our only direct samples of ancient ore-forming solutions (for example, Wilkinson, 2001).

This paper presents the results of a study to develop and apply the new technique of 213 nm UV laser ablation ICP-MS for the quantitative microanalysis of single fluid inclusions. The 213nm system offers improved energy absorption in many geological materials compared to 266 nm UV lasers and also produces a longer pulse width resulting in improved ablation characteristics. A major benefit of this UV system compared to the 193nm ArF excimer laser used elsewhere (Gunther and others, 1997, 1998) is that it does not have the problem of strong absorbance in commonly used optical material such as synthetic fused silica and also air. Beam delivery (through standard UV grade synthetic fused silica optics) and control of the 213nm wavelength is therefore less problematic and expensive (Jeffries and others, 1998).

The laser ablation ICP-MS technique enables the selective, *in-situ* analysis of individual fluid inclusions and under ideal conditions provides multielement data on the chemistry of paleofluids. As such it offers clear advantages over conventional microthermometry, in which only a few components can be estimated, or bulk analyses that may combine multiple fluid inclusion generations or represent a time-average of an evolving fluid chemistry. With good paragenetic control on inclusion chronology, the technique should enable study of the temporal evolution of ore-forming fluids prior to, during, and after ore mineral precipitation.

Quantitative data on the metal content of ore fluids allows the potential link between fluid composition and the metal budget of hydrothermal ore deposits to be evaluated. Currently, the relative importance of reservoir fluid composition, wallrock interaction during fluid transport and selective precipitation in controlling the metal content of deposits is largely unknown. Temporal changes in fluid chemistry associated with precipitation events provide important constraints on the processes that lead to the accumulation of ore-grade concentrations of metalliferous minerals. Finally, determination of the mass of metal precipitated from solution provides an important mass balance constraint on the amount of fluid required to form a deposit and therefore on the validity of numerical flow simulations.

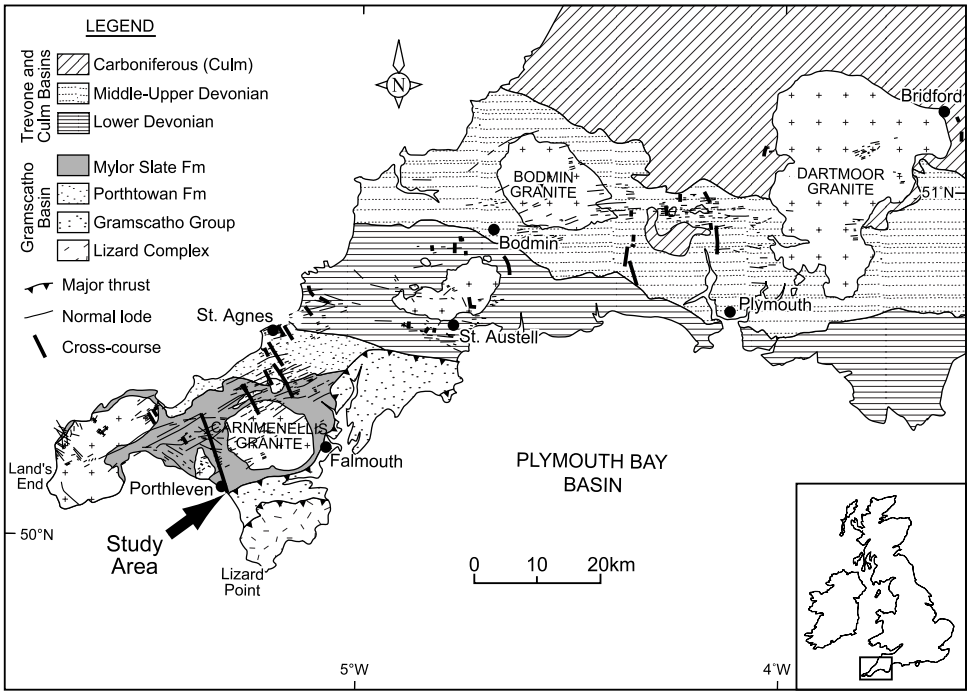

Fig. 1. Location of the sample and study area, showing also the major lithologies.

CASE STUDY: Pb-Zn MINERALIZED VEINS, SOUTHWEST ENGLAND

Background Geology

The Cornubian metallogenic province represents one of the most extensively studied mineralized areas in the world. The geology of the district is dominated by the early Permian Cornubian granite batholith, exposed as a broadly linear array of five major plutons extending for over 220 km through Cornwall and Devon (fig. 1). The batholith was intruded into lowgrade metasediments in multiple intrusion events over a period of about 30 My, each of which was associated with its own phase of hydrothermal activity (Chesley and others, 1993). The granites and their Upper Paleozoic country rocks host the classic granite-related Sn-W(-Cu) hydrothermal deposits for which the district is famous (Dines, 1956; Willis-Richards and Jackson, 1989; Jackson and others, 1989), with most metal production having come from large, east-west-trending veins or 'lodes'.

The district also hosts a suite of N-S to NW-SE-trending mineralized 'crosscourse' veins that postdate the granite-related ores. The crosscourse fissures are up to 7 m wide and are commonly clay-filled due to comminution of the country rock. Where mineralized, the main constituent is banded white quartz, locally occurring with carbonates, barite or fluorite. In several localities (St Austell and St Agnes districts; fig. 1) the crosscourses were exploited for ores of lead, zinc, silver, antimony, arsenic and iron. Small amounts of cobalt, nickel and uranium have also been documented. Dines (1956) divided the crosscourse veins into six general types: Ba-, Pb-, Sb-, U-, Fe-, and Au-bearing veins, associated with quartz, carbonate, jasper, fluorite and hematite.

Scrivener and others (1994) dated fluid inclusions in crosscourse quartz using a Rb-Sr technique, and suggested a Triassic age of 236 ± 3 Ma. Fluid inclusion analyses indicated that the ore-forming brines were derived from evaporated seawater, consistent with fluid generation during deposition of Triassic marine evaporite-bearing sequences (Gleeson and others, 2001).

Fluid inclusion microthermometry has shown that the fluids responsible for crosscourse mineralization were low temperature, high salinity NaCl-$CaCl_2$-H_2O solutions (Alderton, 1978; Wilkinson, ms, 1990; Wilkinson and others, 1995; Gleeson and others, 2000, 2001) similar to those recorded in the Mississippi Valley-type Pb-Zn deposits of the central US (Roedder, 1967, 1976). Geological, geochemical and isotopic evidence, including the presence of low temperature brine fluid inclusions in quartz-anhydrite veins sampled from petroleum exploration wells drilled offshore (Gleeson and others, 2000), suggests that these fluids were basinal brines, expelled from the red-bed dominated Permo-Triassic basins that developed adjacent to the Cornubian high during post-Variscan relaxation (Shepherd and Scrivener, 1987; Wilkinson and others, 1995; Gleeson and others, 2000, 2001).

This basin system is collectively known as the Western Approaches Trough and includes the Melville basin, the St. Mary's basin and the Plymouth Bay basin (fig. 1). These basins consist of tectonised Variscan basement overlain by Permo-Triassic sedimentary fill, which in places reaches thicknesses in excess of 9km (Evans, 1990). From their inception until late Triassic time, the basins were above or temporarily only slightly below sea level, and redbeds dominate the fill sequences. Extensive, Early Permian basal volcanics pass upward into breccias and conglomerates that include volcanic clasts. These rocks fine upwards into red, calcareous and anhydritic siltstones, overlain by reddish-brown sandstones with hematite and calcite cements commonly developed. This unit is overlain by a thick clastic redbed sequence consisting of red arkose and quartz arenite. Above the sandstones is a sequence of grayish-red silty claystones that contain anhydrite, as nodules and in veins. This sequence is overlain by extensive Triassic evaporites, which reach 500m in thickness in places (Evans, 1990).

Mineralizing brines are thought to have migrated laterally from the basins now preserved offshore into adjacent fractured Upper Paleozoic basement, particularly exploiting N-S and NNW-SSE fault and fracture systems (fig. 2). Locally, at fracture-intersections, mixing with heated, meteoric-dominated solutions circulating in EW-trending extensional fault zones occurred (Wilkinson, ms, 1990; Gleeson and others, 2000, 2001).

The crosscourse sampled in this study is situated on the west coast of the Lizard Peninsula in southwest Cornwall, 1 km south of the fishing port of Porthleven (fig. 1). The crosscourse is hosted by the late Devonian Mylor Slate Formation that is made up of dark gray and gray green carbonaceous slates, interbedded with thin bands of pale gray siltstone and sandstone. Immediately to the south lies the Portscatho Formation, part of the middle-late Devonian Gramscatho Group, which consists of fine- to medium-grained sandstone turbidites, interbedded with thin dark gray mudstones. These rocks were deformed and metamorphosed to pumpellyite-actinolite facies during the Variscan Orogeny (Barnes and Andrews, 1981; Wilkinson, ms, 1990).

The main crosscourse structure trends NNW-SSE, is approximately 1 m wide, and is exposed at low tide on the foreshore (fig. 3) depending on the level of the beach sand. The vein primarily comprises rhythmically-banded quartz and minor chalcedonic silica and siderite. Locally, the host rocks are brecciated and silicified and are cut by a number of vein splays, generally sub-parallel to the main structure. Mineralization consists of minor wallrock-hosted arsenopyrite, early chalcopyrite and sphalerite and later abundant galena that forms cubic crystals up to 2cm in size. Previous studies of

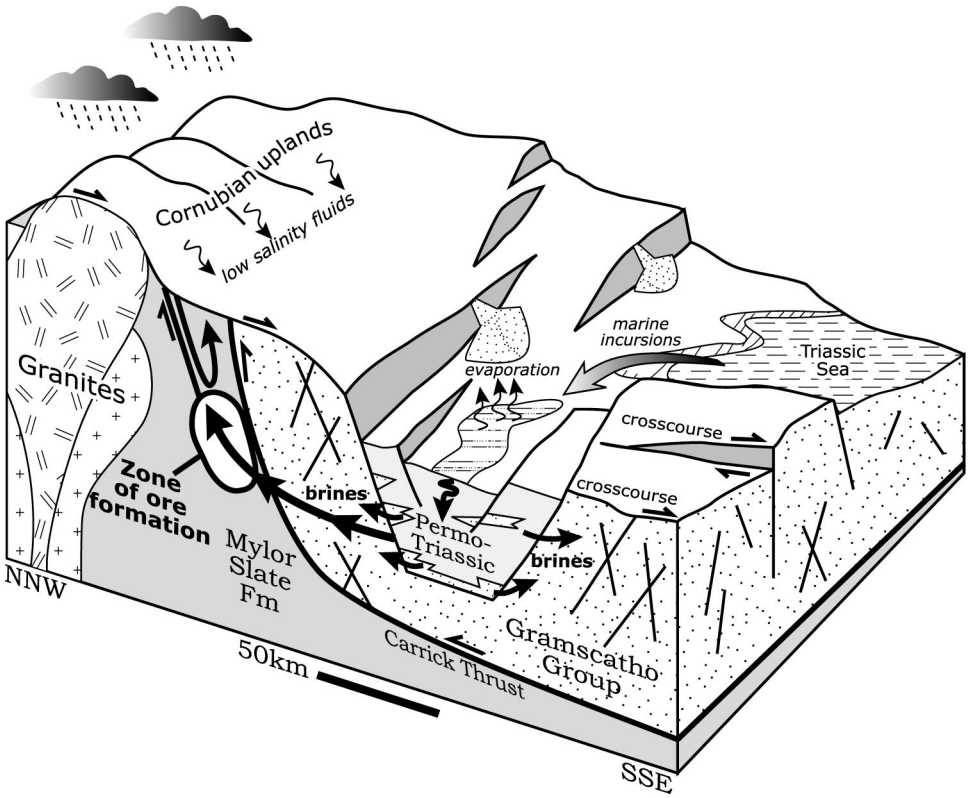

Fig. 2. Schematic block diagram of the orefluid source and migration path in the Triassic (adapted from Gleeson and others, 2001).

this vein also identified quartz-hosted microscopic inclusions of anhydrite (Gleeson and others, 2000; fig. 4A) and K-mica (Wilkinson, ms, 1990; fig. 4B).

METHODOLOGY

Microthermometry

Fluid inclusions were analyzed using a Linkam™ THMSG600 heating-freezing stage, employing standard laboratory procedures (Shepherd and others, 1985). Stage calibration was carried out at −56.6, 0.0, +10.0, +30.4 and 294°C using synthetic H_2O-CO_2 fluid inclusion standards. Measurement precision was generally ± 0.1°C and estimated accuracy was ± 0.2°C in the range −60 to +200°C. The temperatures of ice melting, hydrate melting and liquid-vapor homogenization were measured in all inclusions. First (eutectic) melting was recorded in the larger inclusions in which it could be observed more easily. Measurements of phase transitions were normally duplicated to ensure reliable data were obtained.

Laser Ablation ICP-MS Microanalysis of Fluid Inclusions

Laser ablation was carried out using a New-Wave UP213AI, 213 nm aperture-imaged laser ablation system (Jeffries and others, 1998) equipped with beam homogenization optics. Ablated particulate material was analyzed by a Thermo Element

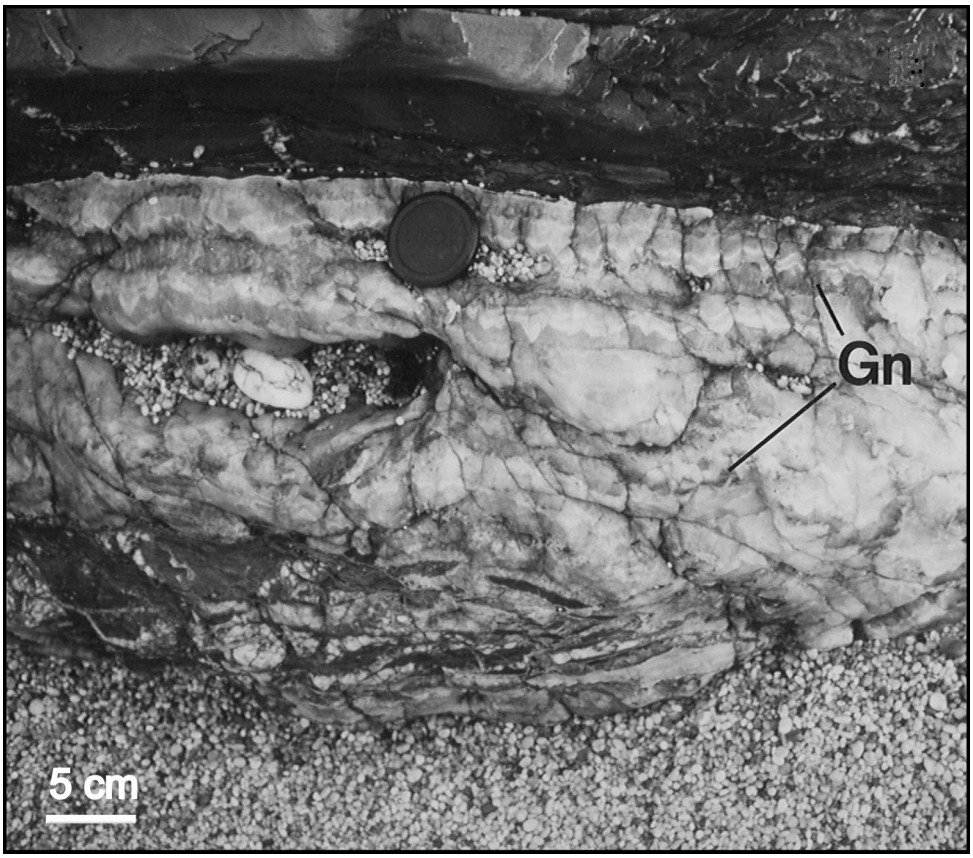

Fig. 3. Field photograph of sampled crosscourse, exposed on the beach near Porthleven.

PlasmaQuad 3 ICP-MS with enhanced sensitivity S-option interface, housed in the Natural History Museum, London. The transport gas was a mixture of He and Ar, at flow rates of 1.1 and 0.7 l min^{-1} respectively. Previous work (Günther and Heinrich, 1999) has demonstrated that the use of a mixed carrier gas significantly improves the transport of the aerosol and reduces fractionation. Tests showed that stable ablation, critical for reproducible analyses, was best achieved by focusing the beam at the sample surface and gradually increasing laser output energy with a constant repetition rate of 20 Hz. Ablation of the mineral surface began at around 0.003 mJ (2.5 J cm^{-2}) after which output energy was gradually increased to 0.03 mJ (24 J cm^{-2}). Output energy was then held constant until fluid release was achieved. This technique enabled a smooth, cylindrical hole to be drilled down to the inclusion of interest, with an optimum pit diameter for stable ablation of ~13 μm. When the inclusion cavity was breached, fluid could be seen to drain from the inclusion over a period of several seconds. The emptied inclusions appear dark due to the increased refractive index contrast between quartz and gas. In every instance, the entire contents of the inclusion cavity were removed by this method, as far as was visible during ablation. Using this approach, multielement data were obtained for inclusions as small as 4.7 × 6.4 μm in the two observed dimensions, and also for inclusions as deep as 80 μm beneath the sample surface. Although no clear evidence of fractionation effects during inclusion

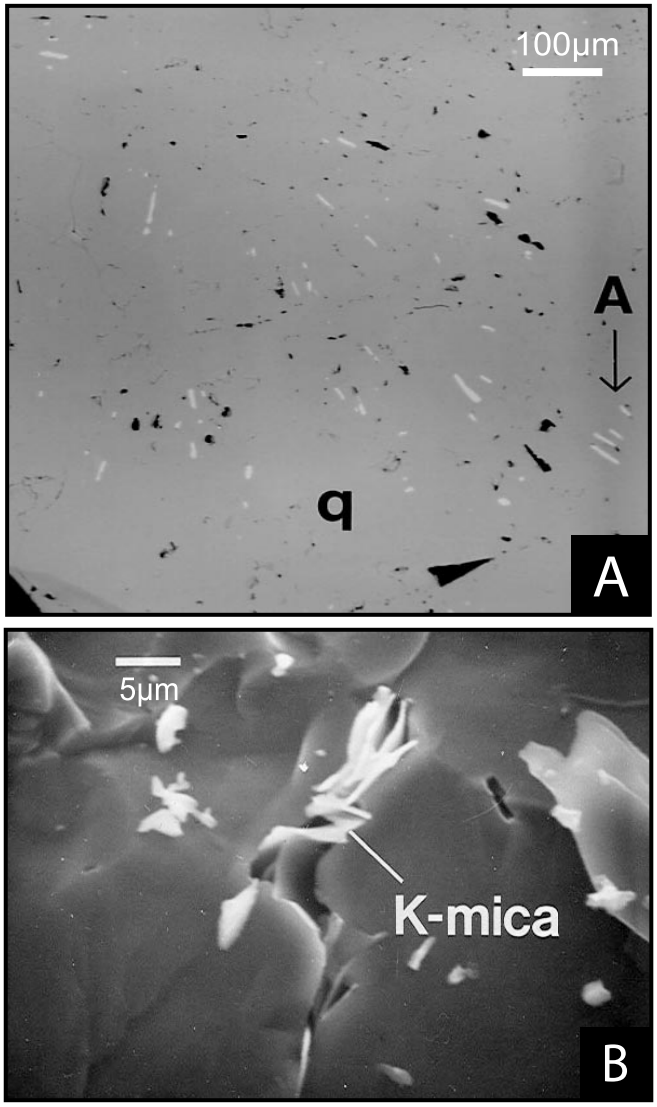

Fig. 4. **A:** back-scattered electron SEM photograph of small anhydrite inclusions (A) in quartz (Q) (Gleeson, ms, 1997), **B:** Secondary electron SEM image of abundant K-mica flakes in irregular fluid inclusion in quartz from growth zone in crosscourse vein exposed at Porthleven (Wilkinson, ms, 1990).

ablation at significant depth was observed in the present study, this possibility requires further evaluation.

Calibration Strategy and Quantification of Element Concentrations

Calibration was carried out at the beginning and end of each experimental run by ablating in duplicate a pure silica glass capillary (external diameter 350 µm, internal diameter 250 µm and 10 mm in length) completely filled with a standard multielement solution. The laser beam diameter used was 13 µm, the same as that used for the inclusion analyses. This approach is broadly similar to the technique described in

greater detail by Ghazi and others (1996) and McCandless and others (1997) and was adopted because it provides a good procedural and matrix-matched analogue for the inclusion ablation process. The capillaries in our study were tipped with molten wax, which upon cooling provided an effective seal preventing any fluid loss from the ends of the tubes.

Figure 5A shows a typical time-resolved signal for ablation of a capillary standard. The initial signal represents the instrumental gas background. Ablation of quartz started at ~38 seconds, marked by a rise in ^{44}Ca (due to a mass interference inferred to be from $^{28}Si^{16}O$) and fluid release occurred at ~58 seconds, indicated by a very large increase in signal intensities (typically 3-4 orders of magnitude). Monitoring of ^{28}Si showed that negligible quartz was ablated during sampling of the fluid itself so the SiO interference on ^{44}Ca is unlikely to be significant with respect to the determination of Ca using this isotope. This conclusion is supported by the good correlation observed for integrated intensity ratios between ^{44}Ca and ^{43}Ca.

Ablation of solution standards was preferred to a NIST glass standard due to a better matrix match with natural inclusions. Preliminary experiments indicated significant differences in element sensitivity between glass and solution ablation processes. Furthermore, the total salinity and concentration of minor elements in the multi element solution can be broadly matched to the natural inclusion fluid, based on microthermometric results and previous bulk fluid inclusion analyses. This approach is likely to minimize potential differences in fractionation behavior between ablation of the standard and ablation of the fluid inclusions.

Figure 5B shows a typical time-resolved signal for fluid inclusion ablation (inclusion no. 32, 43 × 45 μm; 158000 ppm Cl, 95500 ppm Na, 13500 ppm K, 6010 ppm Ca, 1490 ppm Br, 460 ppm Mg, 20 ppm Zn, 6 ppm Ba, 4 ppm Pb). Fluid release occurred at ~59 seconds, approximately 10 seconds after the laser was turned on, and the fluid signal is observed for approximately 12 seconds. A time interval corresponding to the period of quartz ablation prior to fluid release (a "quartz background") was integrated to obtain a background count-rate for each element, which was then subtracted from the fluid inclusion signal. After background subtraction, this signal (in raw counts-per-second) was integrated and converted to equivalent concentrations units using the external standard (compare, Gunther and others, 1998). The limit of detection in the present study was taken as 10 times the standard deviation of the variation of the quartz background signal.

Chloride concentration, independently estimated from microthermometric measurements using the ternary system NaCl-$CaCl_2$-H_2O (Borisenko, 1977), was used as an internal standard for each inclusion to enable calculation of absolute concentrations of the other elements. This is necessary because the total mass of fluid released from a given inclusion during ablation is unknown. Previous workers (Günther and others, 1998) used ^{23}Na as an internal standard. However, we preferred ^{35}Cl due to a high background for Na on the system used and because the estimation of Na from microthermometric data requires significant correction for contributions from other dissolved cations (Heinrich and others, 2003). These could include K and Ca, both of which are present as major elements in many crustal fluids, including those analyzed here.

Experimental Approach

To study the temporal evolution of the orefluid, 49 unambiguously primary inclusions of well-defined relative chronology were selected. Inevitably, the relative ages of inclusions separated by tens of microns in the same growth stage could not be established with complete certainty, but their exact temporal relationship is not important for resolving changes in fluid composition on the observation scale of interest.

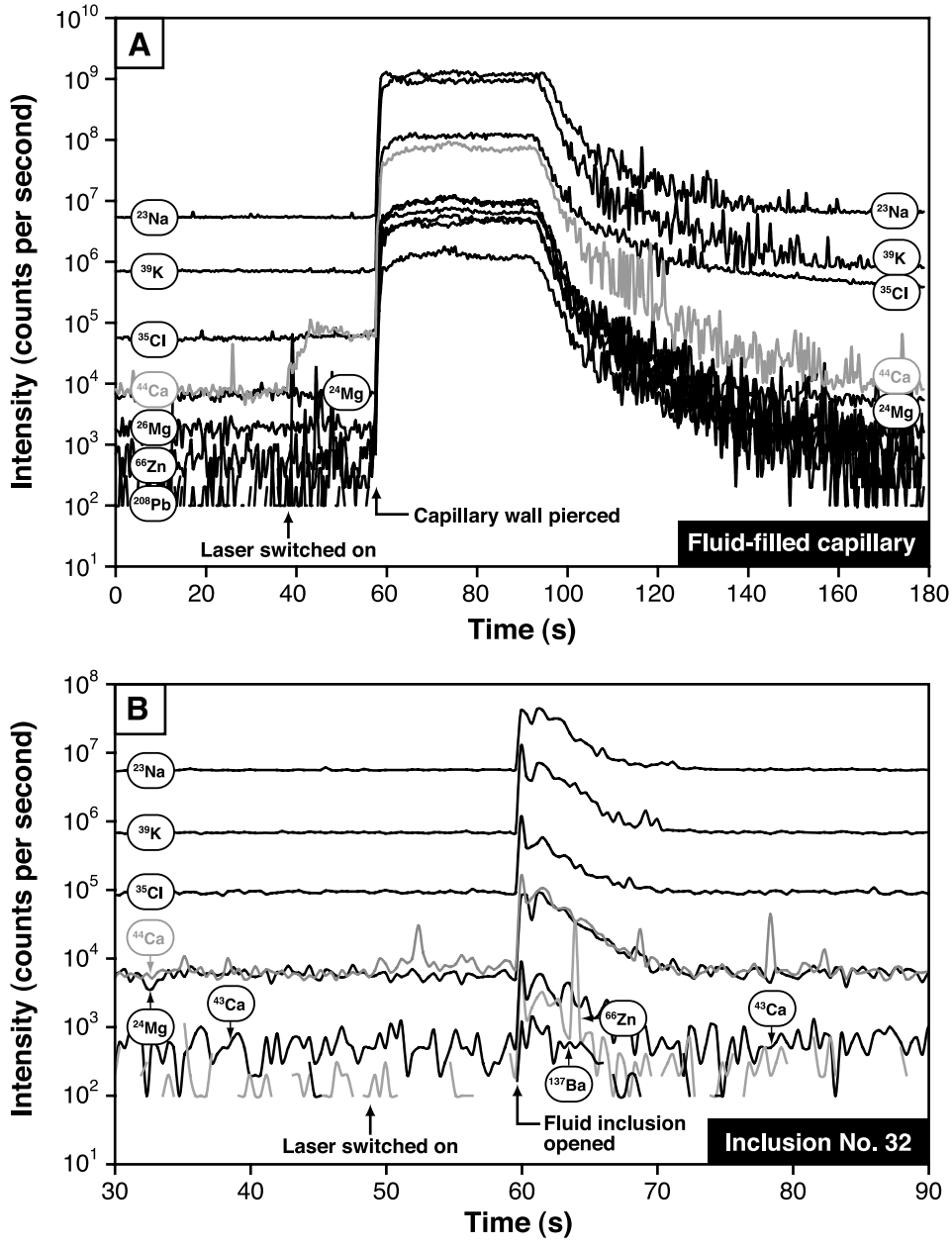

Fig. 5. **A**: Time-resolved release profile for a pure quartz glass capillary filled with a nominal 10 weight percent NaCl solution standard spiked with 30 elements of interest. **B**: Time-resolved release profile for a typical primary fluid inclusion (inclusion no. 32, 43×45μm; 158000 ppm Cl, 95500 ppm Na, 13500 ppm K, 6010 ppm Ca, 460 ppm Mg, 20 ppm Zn, 6 ppm Ba). Time scale is condensed for clarity. Fluid release occurs at ~59 seconds, and the signal is observed for approximately 12 seconds.

As a measure of the reproducibility of the technique, four groups or trails of cogenetic inclusions, each containing 3 to 6 inclusions (18 in total), were analyzed. These inclusions were all secondary in origin with the exception of one group of

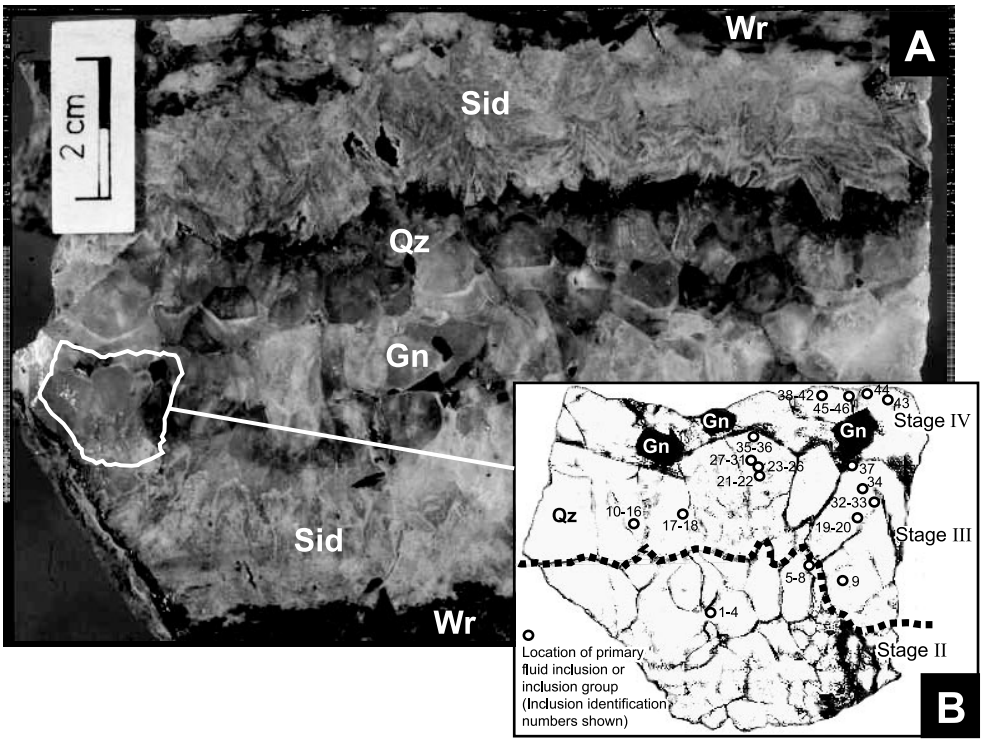

Fig. 6. **A:** Photograph of slabbed vein sample. The vein comprises several stages of growth, symmetrically developed around a central median line. Wr = wall rock, consisting of slate and brecciated (metamorphic) quartz, Sid = siderite, Gn = galena, Qz = quartz. **B**: Enlarged image of fluid inclusion wafer used. Stages (II – V) of vein growth referred to in the text are shown, as are locations of groups of inclusions analyzed. The dashed line marks the boundary inferred to represent a hiatus in vein growth between Stages II and III.

primary inclusions that were very closely spatially related. To assess reproducibility using this approach we have to assume that a tight cluster of inclusions (< 1 inclusion diameter apart) will represent an instantaneous and representative sampling of a homogeneous fluid phase. Although this cannot be proved unequivocally it is a reasonable assumption to make and is supported by the small ranges in microthermometric properties determined for these inclusion groups that are significantly less than for the dataset as a whole.

RESULTS

Sample Petrography

Transmitted light microscopy, fluid inclusion microthermometry and laser ablation ICP-MS analyses were carried out on a 15cm-thick Pb(-Zn) mineralized siderite-quartz vein that forms an offshoot from the main crosscourse structure at Porthleven. This sample was selected because it displays a simple and complete vein growth history within which several distinct stages can be resolved. The sample can be broadly divided into four episodes of vein growth, symmetrically developed around a central median line (fig. 6A). The vein margins are characterized by tan, zoned siderite that forms bladed crystals growing inward from the vein walls (Stage I). This is followed by a thin zone of small, roughly equant, granular quartz crystals (Stage II), overgrown by larger,

transparent quartz crystals, elongated in the direction of crystal growth (Stage III). The boundary between Stages II and III is very conspicuous in hand specimen and thin section and may represent a hiatus in quartz deposition. The large crystals in Stage III contain well-developed growth zones, defined by abundant, irregular primary fluid inclusions, the most distinctive of which is immediately followed by sporadic galena crystals. This zone also contains microscopic (<10 μm) flakes of a birefringent phase, probably K-mica (for example, fig. 4B). A final phase of euhedral quartz deposition concludes the vein growth history (Stage IV).

The 150 μm thick doubly-polished wafer prepared for analysis represents a section across one half of the vein (fig. 6B). This sample was selected as a representative example of growth stages II-IV allowing a relatively complete history of fluid evolution during quartz precipitation to be studied. In particular, the sample spans the main galena precipitation horizon within the vein, enabling fluid chemical changes prior to, during and after sulfide mineralization to be evaluated.

Inclusion Petrology

Abundant two-phase (liquid + vapor) aqueous inclusions averaging ~23 × 9 μm in two dimensions are present. The distribution of inclusions within the sample is such that most primary inclusions, defined according to the criteria of Roedder (1984), occur within or close to growth zones, with large areas of the quartz crystals relatively inclusion-free. Primary inclusions are distributed typically in random 3-D groups and are often elongated in the direction of growth. Occasionally, isolated inclusions are observed (fig. 7A). The primary inclusions selected for analysis occur in groups throughout Stages II-IV of the vein sample (fig. 6B). They are considered to provide a fairly complete record of fluids present during vein formation.

Secondary inclusions typically occur in planar groups or trails, outlining healed fractures, and tend to have a flatter, more irregular shape than the primary inclusions (fig. 7C) although small, equant, secondary inclusions are also observed (fig. 7D). Fluid inclusions in siderite (Stage I) were too small for microthermometric analysis.

Microthermometry

Microthermometric results are in good agreement with previous work on cross-course fluids (for example, Gleeson and others, 2000). First melting generally occurred at −52 to −53°C, comparable with the ternary eutectic for the system NaCl-$CaCl_2$-H_2O (Borisenko, 1977; Oakes and others, 1990). Most inclusions (95%) showed equilibrium ice melting between −21 and −25°C (mode −23.6°C). Hydrohalite was the final phase to melt at −0.1 to +12.1°C (mode +5.0°C), persisting to higher temperatures than predicted by phase equilibria in the NaCl-$CaCl_2$-H_2O system. All fluid inclusions homogenized to the liquid phase between 81.2 and 195.7°C (mode 126°C), although the majority (80%) were in the range 120 to 145°C (table 1). The few significantly lower or higher values are likely to be due to necking-down prior to nucleation of the vapor bubble.

The microthermometric data mostly fall in a narrow range (table 1) that could be taken as evidence of a fairly stable hydrothermal system with limited chemical variability. However, this apparent homogeneity is belied by the laser ablation data that reveal large compositional fluctuations.

Laser Ablation ICP-MS Microanalysis

Laser ablation was successful in opening and releasing fluid from all fluid inclusions mapped, and all ablations yielded a detectable signal for at least six elements. The majority of the ablation pits were characterized by a smooth-sided, cylindrical geometry (fig. 7E) with no residual solids evident within or around them. Some pits showed minor sharding of the quartz at the surface from the first stage of the

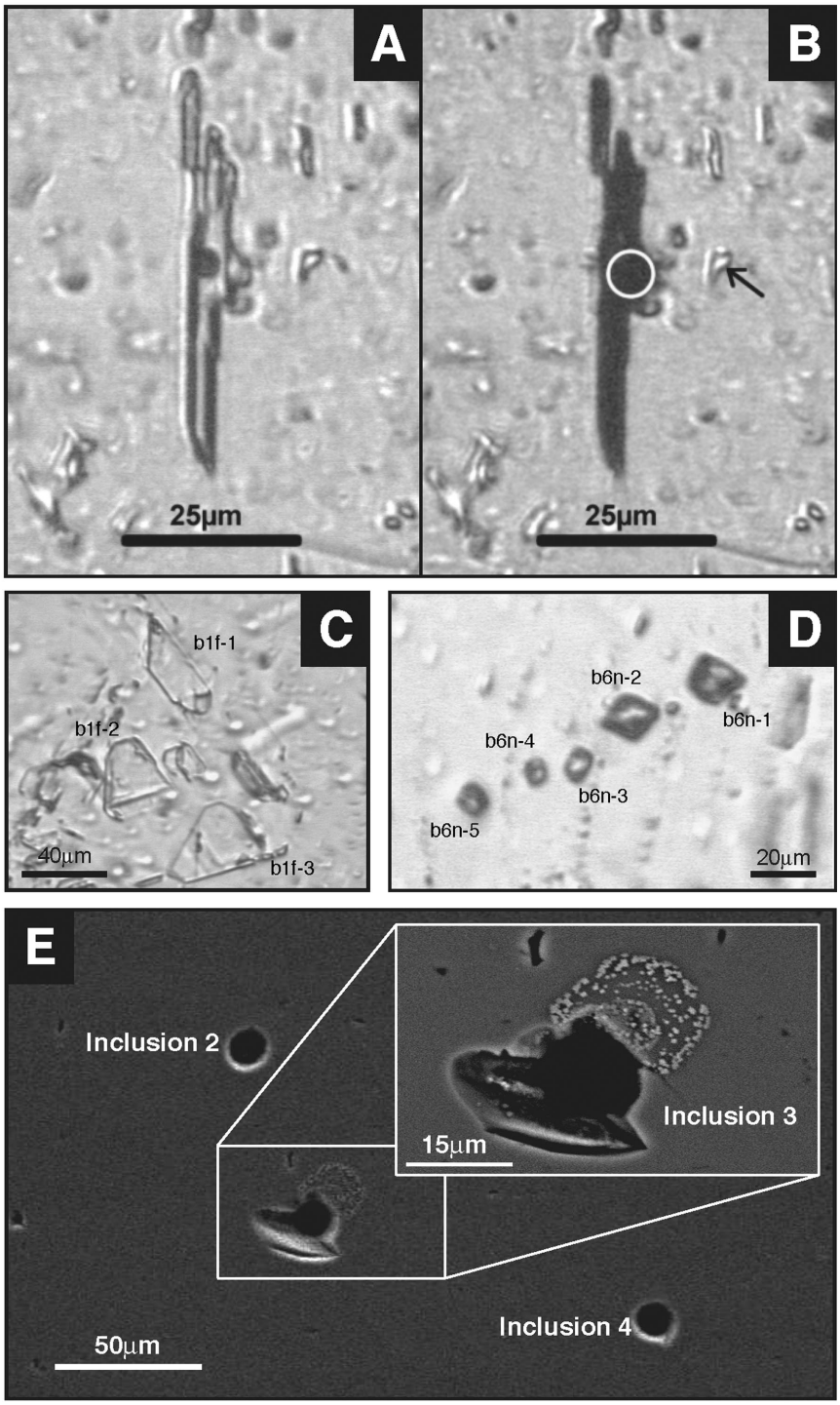

Fig. 7. Photomicrograph of an isolated, primary fluid inclusion **A**: before, and **B**: after, laser ablation. The location of the ablation pit is shown by the white circle. Note small inclusion nearby (arrowed) is unaffected by the ablation process. **C**: A group of planar secondary inclusions occurring on a fracture plane. **D**: A trail of more 3-dimensional secondary inclusions (data for the inclusions shown in **C** and **D** can be found in table 3). **E**: SEM images of ablation pits showing normal cylindrical form, and an example of an inclusion close to the surface that sharded when opened, leaving a residue of Na-Ca-Cl salts.

ablation process, but this generally occurred prior to fluid release. In three instances, fluid inclusion contents were partially spilt on release leaving a solid residue after evaporation (fig. 7E). This residue occurred in association with extreme sharding, which appeared to be related to the very shallow depth of these inclusions. Qualitative EDS analysis detected Ca, Na and Cl in the residue; none of the ore metals of interest were observed. Consideration of the laser data for these poor ablations showed that low Cl, Na and/or Ca values were recorded compared with neighboring inclusions, suggesting that fractionation had occurred. These analyses were therefore rejected from the final dataset and the inclusions are not numbered on figure 6B or listed in the data tables.

The complete dataset for 46 primary inclusions is given in table 1. Resolution of signals above the limit of detection for individual elements (here 10 times the standard deviation of the background variation) is largely a function of inclusion volume for fluids of a similar salinity (Heinrich and others, 2003); therefore, for smaller inclusions, the dataset is necessarily incomplete. The limit of detection values for elements not determined in a particular analysis are also shown in table 1.

The good agreement between the average Ca estimated from microthermometric measurements and the laser analyses, together with the excellent charge balance obtained (table 2) suggests the technique is accurate to within around 10 percent for major element determinations. Geochemical coherence in the results is indicated by the strong correlations between elements that typically behave in a similar fashion such as Ca and Sr ($r = 0.77$), and K and Rb ($r = 0.74$). If the individual analyses are combined to give a time-averaged fluid composition, there is reasonable agreement with previous major element analyses by bulk decrepitation-linked ICP-AES (D-ICP) and halogen ratio determinations obtained by crush-leach analysis (Gleeson and others, 2001; see table 2). These techniques, in which many thousands of inclusions are opened, should give a good average of the entire compositional range measured in the individual inclusion analyses reported here. Of the base and precious metals, only Pb and Zn (and occasionally Sb) were detected at >ppm levels, consistent with the predicted metal transport potential of low temperature saline fluids (for example, Anderson, 1973) and with the sulfide mineralogy of the crosscourse veins in the area. The measured metal concentrations fall in the same range as modern basinal brines (Carpenter and others, 1974; Hanor, 1994).

Temporal Changes in Ore Fluid Chemistry

Figure 8 illustrates the temporal changes in orefluid chemistry revealed by the laser ablation analyses. These variations are summarized below, broken down for simplicity into the stages of vein growth described previously. Stage III has been subdivided into IIIa and IIIb (fig. 8) because of the marked change in fluid chemistry observed in this interval of vein growth. It is important to note that the chronology of the primary fluid inclusions is relative rather than absolute; consequently, the x-axis in figure 8 is not linear.

Stage II.—Element concentrations in the initial stage of quartz growth are somewhat variable and the fluid trapping record is incomplete. Inclusions #1 to 4 are separated from inclusions #5 to 9 by ~3 mm of quartz growth (fig. 6) and these two groups display rather different compositions to each other, particularly evident in the Cl and Ca concentration data (fig. 8). The latter group have compositions that are fairly typical of the suite of analyses as a whole with the ore metals, Pb and Zn, in the range <6 to 27 and <23 to 86 ppm respectively and a Zn:Pb ratio of ~2.

Stage IIIa.—The trace element chemistry of the inclusions in Stage IIIa, after the inferred hiatus in quartz growth, is markedly different from Stage II. Although the temperature and salinity of the fluids have not significantly changed, the brines are highly enriched in Pb (up to 295 ppm) with a very low Zn:Pb ratio of ~0.2. This

TABLE 1

Multielement dataset for the 46 primary inclusions analysed

INC. #		T_h	Sal[†]	Size (μm)[*]	^{7}Li	‡^{23}Na	^{24}Mg	^{35}Cl	^{39}K	^{43}Ca	^{44}Ca	‡^{42}Ca	^{55}Mn	^{66}Zn	^{81}Br	^{85}Rb	^{88}Sr	^{121}Sb	^{133}Cs	^{137}Ba	^{208}Pb
1		122.3	26.2	50 x 21	35	88398	<9	160029	6603	7990	6583	12940	<3	<1	<1160	25	248	212	12	3	29
2	STAGE II	81.2[§]	25.9	48 x 6.6	54	94447	<22	157812	4692	16508	13314	6602	106	34	<2500	29	502	<15	41	9	5
3	STAGE II	124.1	26.0	38 x 15	<112	90763	174	158761	3788	<6789	2055	10242	<32	8	<10300	38	57	<18	18	<9	17
4	STAGE II	132.5	26.0	29 x 7	<142	89920	<76	159107	2038	<11760	10231	11146	<28	<11	<12900	<11	369	153	17	5	34
5	STAGE II	134.3	26.6	139 x 9	<55	86079	367	162825	21314	21548	17580	16437	42	<23	<4470	106	562	<5	53	<30	<6
6	STAGE II	n.d.	26.6	29 x 7	<378	86079	364	162825	13859	<26150	13298	16437	201	86	<26000	105	519	<32	<60	<28	<50
7	STAGE II	113.2	26.7	30 x 9	<68	84633	242	163797	12940	17800	14156	18194	298	53	<4010	93	545	31	38	7	27
8	STAGE II	142.5	26.7	28 x 25	<58	84633	424	163797	12486	14134	12211	18194	54	36	<4800	65	346	5	32	8	21
9		137.3	25.9	78 x 24	<48	94447	164	157812	13370	5694	3467	6602	84	<13	<2860	51	99	16	20	<12	<13
10		123.3	26.8	35 x 17	<38	83923	63	164290	7908	10710	8244	19066	49	22	1806	43	289	<1	21	11	295
11		124.7	27.1	29 x 15	<76	80471	453	166742	4355	10535	9469	23334	55	23	3229	84	394	<3	21	9	266
12		124.8	26.7	11 x 78	<13	84633	50	163797	7214	11420	9859	18194	93	25	462	36	340	1	19	12	153
13		123.3	26.8	87 x 9.6	<24	83221	26	164785	9731	11581	8298	19932	11	28	1385	41	344	<1	22	12	216
14		124.8	27.0	38 x 7	<101	81835	155	165772	5062	8428	7287	21647	62	26	6117	40	266	<5	20	10	257
15	STAGE IIIa	130.0	26.8	35 x 17	<55	83221	<37	164785	7256	12202	9941	19932	114	22	1714	53	358	<3	25	12	29
16	STAGE IIIa	130.0	26.5	42 x 9.6	<38	86818	36	162353	3590	12634	10790	15552	38	16	1985	36	252	<3	26	5	258
17	STAGE IIIa	122.5	27.1	17 x 23	219	81151	323	166260	12631	18587	13882	22494	260	48	<5550	66	470	11	32	21	99
18	STAGE IIIa	122.5	27.2	11 x 22	87	79795	546	167216	4790	21936	7416	24166	58	60	<7800	48	862	9	27	12	<85
19	STAGE IIIa	126.4	26.2	22 x 34	86	88398	<20	160029	8601	21382	20368	12940	<4	<4	1431	29	578	14	24	20	19
20	STAGE IIIa	125.6	26.6	33 x 26	<26	86079	<12	162825	8526	16102	16669	16437	<3	<3	1223	32	627	<1	22	17	20
21	STAGE IIIa	135.4	26.9	37 x 17	207	82525	<84	165280	11658	29686	22879	20792	256	70	<11900	94	657	14	53	13	<6
22	STAGE IIIa	124.9	26.9	18 x 21	<194	82525	198	165280	10899	12151	10265	20792	161	57	<24300	49	299	9	28	13	12
23	STAGE IIIa	126.1	26.8	27 x 15	65	83923	419	164290	14536	25201	18857	19066	259	77	<5070	87	747	8	43	29	21
24	STAGE IIIa	120.4	26.7	30 x 7	<207	84633	360	163796	5968	18642	17655	18194	110	44	<29300	67	478	<9	38	<15	16
25	STAGE IIIa	135.5	26.7	25 x 16	<388	84633	887	163797	13695	32000	19059	18194	211	93	<41200	115	616	<25	52	<12	30
26	STAGE IIIa	135.5	26.7	24 x 11	<326	84633	596	163797	11635	<22480	18438	18194	121	86	<34300	74	507	<12	38	29	51
27	STAGE IIIa	132.8	27.1	13 x 33	<366	81151	508	166260	15270	21568	18903	22494	260	138	<33500	86	505	<30	37	<16	65

TABLE 1
(continued)

INC. #		T_h	Sal†	Size (μm)*	^{7}Li	‡Na	^{24}Mg	^{35}Cl	^{39}K	^{43}Ca	^{44}Ca	‡Ca	^{55}Mn	^{66}Zn	^{81}Br	^{85}Rb	^{88}Sr	^{121}Sb	^{133}Cs	^{137}Ba	^{208}Pb
28		153.6	26.3	25 x 9	241	86863	515	160924	7208	25575	20526	14731	117	67	<30700	73	623	<8	34	11	<10
29		n.d.	26.3	26 x 9	283	86863	562	160924	11517	26216	<19790	14731	127	46	<28400	91	595	<120	36	<6	17
30	STAGE IIIb	123.0	26.8	11 x 15	67	83923	261	164290	13533	19566	15217	19066	173	68	<6350	67	433	4	28	16	30
31		158.3	26.2	65 x 19	134	87625	169	160470	13091	23175	19550	13836	115	76	<2750	83	554	<1	34	9	4
32		133.3	25.9	43 x 45	112	95466	457	157711	13500	4456	6006	5684	66	20	1488	81	116	4	28	6	4
33		131.0	26.0	125 x 56	<23	100103	163	158047	12855	3900	4272	1942	15	10	1413	72	97	9	25	5	1
34		146.0	25.9	85 x 30	<40	97658	169	157716	6943	2035	2914	3830	21	13	2123	38	57	<1	12	1	3
35		126.5	27.4	33 x 17	<113	77793	<146	168583	2715	25115	20473	26611	<65	<100	<11000	<49	1396	22	<64	26	55
36		98.0§	26.9	20 x 20	<108	82525	<79	165280	4517	41334	33690	20792	26	<29	<15000	<13	962	26	36	12	15
37		144.8	23.1	8 x 10	<33	85023	<36	140441	9389	17467	15423	5052	<7	8	3487	30	465	8	29	17	19
38		121.8	27.5	63 x 8	304	77331	569	169263	14115	22518	17439	27375	239	67	<4030	67	531	11	28	9	32
39		125.1	27.5	27 x 13	748	76602	590	169594	8671	33467	20114	28174	224	87	<12200	85	587	<13	42	12	36
40	STAGE IV	125.1	27.5	3.8 x 13	1432	76602	2438	169594	11509	<63700	<20480	28174	345	<129	<85000	97	479	<87	<54	<36	<87
41		139.3	28.0	26 x 4.4	926	71114	452	173096	8682	<31720	13346	34742	279	<52	<33400	74	420	<51	39	14	43
42		136.4	28.0	7.7 x 6	1151	71114	478	173096	9917	<42400	10629	34742	183	<60	<46400	68	374	81	31	<24	<36
43		118.5	27.7	75 x 38	17	74882	312	171058	5051	17310	20448	30434	444	40	1083	45	607	1	20	15	36
44		120.7	26.6	26 x 20	<57	85352	<17	163308	537	16039	14868	17318	<9	<5	2293	<2	470	<2	11	6	13
45		130.9	27.5	16 x 4.4	<328	76602	<161	169594	2728	20970	19063	28174	<51	<42	<23800	<26	488	90	<13	12	981
46		110.9	27.5	23 x 4.8	<655	77331	<542	169263	4455	57677	26450	27375	173	<48	<35200	<48	816	<57	<19	18	<40

†The total salinity as total NaCl + $CaCl_2$ wt% equivalent. *Dimensions of the inclusion in plan view. §Inclusion possibly necked-down.
‡Na and ‡Ca are the microthermometric values. <indicates analyte below detection limit of 10 times the std. dev of the background. n.d.: not determined.

TABLE 2

Summary of fluid inclusion compositional data (ppm) and comparison with previous bulk analyses of vein samples from the same locality and contemporary basinal brines.

Element	Range	Mean	D-ICP[†]	D-ICP[Ψ]	Oil Field Brines[§]
Cl	140000-175000[¥]	164000[¥]	156000[¥]	165000[¥]	132000
[‡]Na	71100-100100[¥]	84200[¥]	78600[¥]	82900[¥]	49700
[‡]Ca	1900-35000[¥]	19000[¥]			
^{43}Ca	2000-58000	18000	19400	21000	26800
^{44}Ca	2100-34000	14200			
K	500-21300	9500	10100	8440	1870
^{81}Br	460-6120	2080	n.d.	910*	n.d.
^{79}Br	300-2210	1000			
Sr	50-1400	450	370	n.d.	1340
^{26}Mg	45-1500	440	n.d.	360	2030
^{24}Mg	25-2500	400			
Li	15-1400	280	83	n.d.	n.d.
Mn	10-350	160	95	n.d.	n.d.
Pb	<1-350	90	n.d.	n.d.	20
Rb	15-115	60	n.d.	n.d.	n.d.
Zn	5-150	50	n.d.	n.d.	100
Cs	7-53	28	n.d.	n.d.	n.d.
Sb	<1-210	25	n.d.	n.d.	n.d.
Ba	1-29	11	28	n.d.	43
Charge balance (based on ^{44}Ca)		-0.8%			
Charge balance (based on ^{43}Ca)		+4.3%			

[‡]Ca and [‡]Na values estimated from microthermometric data, assuming hydrohalite melting at 0.1°C. [¥]Estimated from low temperature phase equilibria in the NaCl-$CaCl_2$-H_2O model system (Oakes et al., 1992). [†]Mean of decrepitation-linked ICPAES bulk analyses reported by Wilkinson (1990). [Ψ]Mean of decrepitation-linked ICPAES bulk analyses reported by Gleeson et al. (2001) corrected for error in reported Cl concentration. *Determined by crush-leach bulk analysis. [§]Mean of data reported by Carpenter et al. (1974). The elements Cr, Fe, Co, Ni, Cu, Br, Mo, Ag and Au were all below detection in the majority of inclusions. n.d.—not determined.

chemistry remains steady for several analyses until inclusion #15, after which the Pb concentration falls sharply to <6 ppm across several inclusions. At this point, a small apparent increase in Zn concentration (though within the uncertainty of the measurements), is followed by a significant drop to <3 ppm. This drop coincides with a transient decrease in Cl concentration of around 7000 ppm (4%). In the final part of Stage IIIa, both Pb and Zn concentrations increase together, with the Zn:Pb ratio returning to values similar to the end of Stage II (~3). Other elements (K, Sr, Ba) show gradual and fairly systematic concentration increases of up to an order of magnitude through Stage IIIa. The laser ablation Ca data also show this trend, although it is not observed in the estimate of Ca based on microthermometric measurements suggesting that the ternary phase equilibria do not accurately predict Ca concentrations for the entire range of fluid inclusion compositions studied.

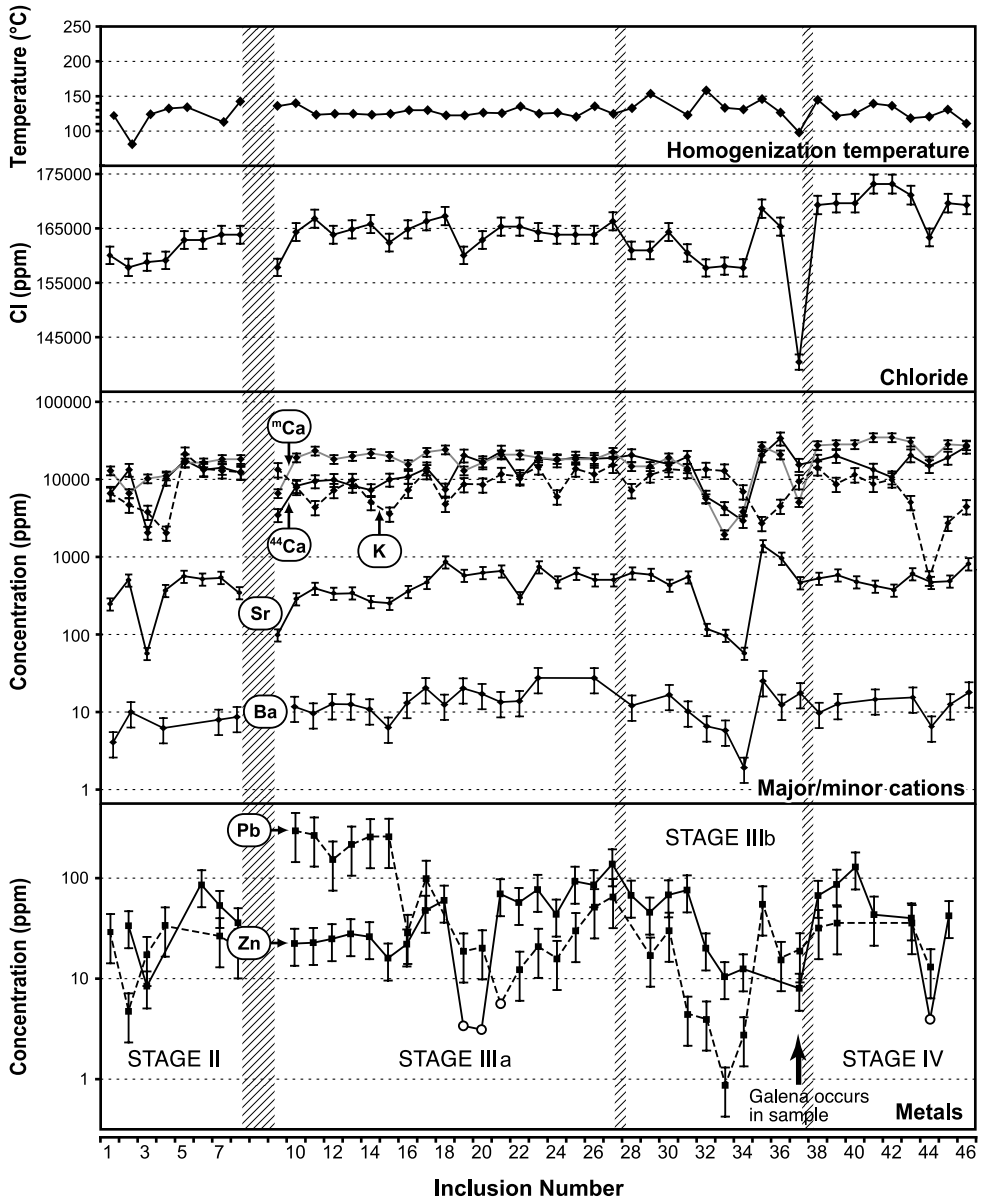

Fig. 8. Four main stages of evolution of fluid chemistry determined by analysis of temporally constrained primary fluid inclusions. Error bars represent average reproducibility (relative standard deviation) for each element based on analyses of cogenetic fluid inclusions. Error on Cl estimated from uncertainty in microthermometric measurement. Open circles indicate a detection limit rather than an actual value, and represent maximum possible concentrations.

Stage IIIb.—The most significant changes in fluid chemistry are observed in Stage IIIb that represents quartz growth immediately prior to the most prominent growth zone and the sulfide precipitation horizon within the sample. Broadly synchronous decreases of up to two orders of magnitude in the concentrations of K, Ca, Ba, Sr, Pb and Zn are observed. Up to 98 percent of the Pb and 94 percent of the Zn are

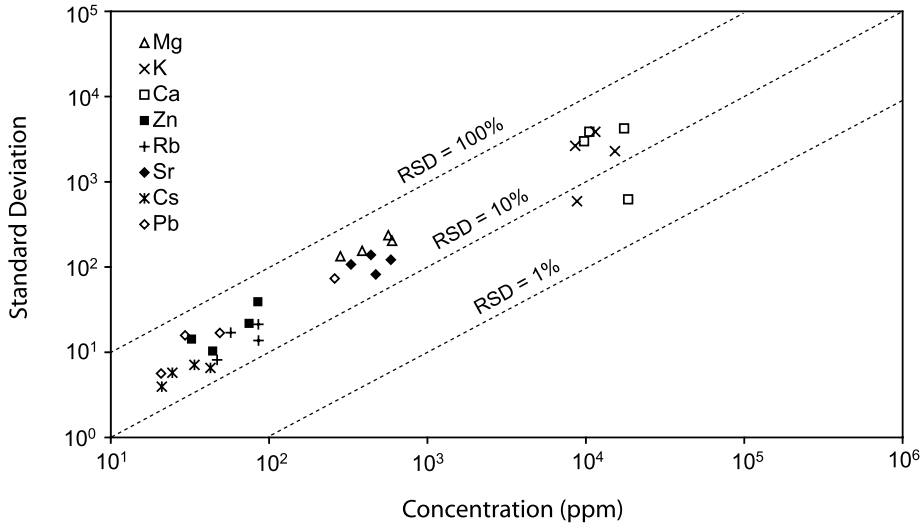

Fig. 9. Analytical reproducibility for laser ablation ICP-MS analysis of fluid inclusions. Each datapoint represents a relative standard deviation value determined for one element on a group of cogenetic fluid inclusions (four groups analyzed in total). Note lack of relationship between RSD values and concentration.

apparently lost from solution during this interval. Closer examination of the trends reveals that Ba, Pb, and Zn start to decrease first (at #27-32) followed by Ca and Sr (at #32) and K (at #34). These decreases correspond to a drop in fluid salinity of around 5 percent as indicated by the Cl data (fig. 8). A return to higher salinities at #35 to 36 is mirrored by increases in Ca, Sr, Ba and Pb but K appears to behave independently, remaining suppressed until #37. A single inclusion (#37), displaying the largest drop in salinity of all, shows low Ca, Sr, Zn and Pb values. This drop marks the appearance of galena in the sample and concludes Stage IIIb.

Stage IV.—Stage IV sees a return to values close to those characteristic of the latter part of Stage IIIa. Zn and Pb concentrations are at the tens of ppm level and Zn:Pb ratios are in the range 1.1 to 2.4. Concentrations of Cl, Ca, Sr, and Ba vary little through the stage with the exception of a coincident drop in salinity, K, Pb and Ba at #44.

Reproducibility

Reproducibility data for selected elements in the four groups of cogenetic inclusions analyzed give mean relative standard deviation (RSD) values equal to or less than 25 percent for calculated K, Ca, Rb, Sr and Cs concentrations (fig. 9 and table 3). RSD values for Mg, Pb and Zn are in the range 30 to 50 percent. These are comparable with previous work conducted using different experimental procedures (Günther and others, 1997), and are more than sufficient to resolve the observed natural concentration variations of over two orders of magnitude. No correlation between RSD and concentration is apparent (fig. 9); this lack of correlation can be attributed to the wide variation in instrumental sensitivity of the elements analyzed.

DISCUSSION

Too few data are available from Stage II to make substantive conclusions for this interval. A significant change in fluid chemistry is implied by the marked difference in major element chemistry of the inclusion groups trapped early and late in the stage but this change has not been adequately documented by the inclusions analyzed.

TABLE 3

Reproducibility data for selected elements derived from groups of cogenetic inclusions

Inclusion	T_h (°C)	Sal	^{24}Mg	^{39}K	^{44}Ca	^{66}Zn	^{85}Rb	^{88}Sr	^{133}Cs	^{208}Pb	Size* (μm)
b1j-1	128.2	26.8	419	14536	18857	77	87	747	43	21	33 x 17
b1j-2	125	26.7	360	5968	17655	44	67	478	38	16	30 x 7
b1j-3	137.6	26.7	887	13695	19059	93	115	616	52	30	25 x 16
b1j-4	124.7	26.7	596	11635	18438	86	74	507	38	51	24 x 11
Mean	129.3	26.7	565	11458	18502	75	86	587	43	29	
Std. Dev	7.3	0.03	237	3858	622	22	21	122	7	16	
RSD (%)			**42**	**34**	**3**	**29**	**25**	**21**	**15**	**54**	
b1f-1	151.4	26.9	434	8107	12876	48	56	292	20	343	44 x 31
b1f-2	157.4	26.9	181	9122	6911	20	45	245	25	230	64 x 21
b1f-3	141.1	26.6	231	9145	9464	29	40	449	18	205	27 x 14
Mean	150.0	26.8	282	8791	9750	32	47	329	21	259	
Std. Dev	6.7	0.19	134	593	2993	14	8	107	4	74	
RSD (%)			**47**	**7**	**31**	**44**	**17**	**33**	**19**	**28**	
b6n-1	127.7	26.5	490	14710	18638	55	75	498	26	21	19 x 19
b6n-2	129.5	26.1	588	16025	16689	60	87	453	31	20	17 x 18
b6n-5	129.3	26.6	377	18255	20503	72	82	509	39	16	10 x 9.5
b6n-4	131.2	26.1	921	15296	10476	151	108	340	29	17	7.5 x 6.7
b6n-3	148.2	26.1	613	11934	20872	87	75	556	43	30	11 x 8
Mean	133.2	26.3	598	15244	17435	85	86	471	34	21	
Std. Dev	8.5	0.25	203	2287	4232	39	14	82	7	6	
RSD (%)			**34**	**15**	**24**	**46**	**16**	**17**	**21**	**27**	
b1a-7	135.2	28.1	156	7783	16322	40	34	649	18	62	18 x 110
b1a-1	135.4	27.0	275	7265	11050	40	52	357	17	29	79 x 44
b1a-2	127	27.0	468	12727	11840	50	69	540	30	49	28 x 47
b1a-3	128.3	27.0	491	11590	10557	34	82	461	29	34	27 x 18
b1a-4	124.5	27.0	512	6801	4534	50	45	284	27	<89	8.2 x 7.8
b1a-5	131.4	27.0	<377	7273	7918	62	59	352	30	67	6.8 x 7.2
Mean	130.3	27.1	380	8907	10370	46	57	440	25	48	
Std. Dev	4.5	0.41	157	2564	3954	10	17	136	6	16	
RSD (%)			**41**	**29**	**38**	**21**	**30**	**31**	**24**	**34**	
Mean											
RSD (%)			**41**	**21**	**24**	**35**	**22**	**25**	**20**	**36**	

<indicates a detection limit rather than a real value and represents a maximum value for that element in that particular analysis. *The size given in microns is the dimensions of the inclusion in plan view. The elements listed are those for which data were obtained from all or most of the inclusions in that group.

The contrast in fluid chemistry between Stages II and IIIa is consistent with some sort of growth hiatus at the boundary and it is suggested that vein growth temporarily ceased and was re-established when a new pulse of fluid invaded the fracture system. The new fluid was significantly enriched in Pb and had a low Zn:Pb ratio.

The most significant change observed in Stage IIIa is the drop in Pb concentration of around an order of magnitude between inclusions #14 to 18 that does not correspond to decreases in any of the other elements. In the absence of evidence for dilution, such a systematic change can only be easily explained by precipitation of a Pb-rich phase, most likely galena. Equilibrium solubility relationships of sulfides in low temperature brines are such that galena precipitation alone can occur only if a fluid is significantly undersaturated with respect to sphalerite (for example, Huston and Large, 1987). Consistent with this possibility is the low Zn:Pb ratio observed at the start of Stage IIIa, which is well below that predicted for saturation with respect to both

sulfides in such fluids (for example, Sverjensky, 1981). Fluid mixing or cooling are unlikely causes of galena precipitation since no changes in salinity or temperature are observed at this point (fig. 8). Given that the ore veins occur close to the basinward contact of the Mylor Slate Formation, the first highly reducing rock unit encountered by fluids exiting the oxidized basin source region (fig. 2), reduction by wall rock reaction is perhaps the most likely process driving galena precipitation in the initial stages of vein formation.

The observed decrease in Zn concentration to below the limit of detection of around 3 ppm at analyses #19 to 20 implies that at this point, precipitation occurred of a Zn-rich phase, presumed to be sphalerite. Pb concentrations continued to decrease over this interval implying continued deposition of galena. The fact that this event coincided with a decrease in Cl, a conservative element, suggests that dilution of the brine (due to fluid mixing) was an additional mechanism driving mineral precipitation at this time. The stabilization of Zn:Pb ratios at around 3 subsequent to this inferred precipitation event can be explained by buffering of the fluid at galena and sphalerite saturation by the presence of these phases in the vein system.

Although sulfide precipitation during Stage IIIa is inferred from the fluid inclusion data, neither galena nor sphalerite crystals are observed in Stage IIIa of the sample studied. This apparent contradiction can be accounted for if precipitation of sulfides occurred upstream, perhaps within the main ore vein, with the fluid inclusions trapping the residual, depleted fluids. If correct, this is an important conclusion because it means that fluid inclusion chemistry can record precipitation events that have occurred elsewhere in hydrothermal fracture networks, a characteristic of potential use in mineral exploration.

Subsequent to analysis #15, fairly systematic increases in Ca, Ba, Sr, K and Zn (excluding the drop at #19 - 20) are observed across ~ 1cm of quartz growth. These increases exceed the analytical uncertainty and probably reflect a real evolution in orefluid chemistry. Comparison with analyses of analogous modern basinal brines from the Mississippi Basin, Northern Gulf of Mexico (Carpenter and others, 1974; see table 2) shows that the inclusion data fall on well-defined arrays that through Stage IIIa trend toward contemporary basin water compositions (fig. 10). The fact that the data do not fall on the predictable trends characteristic of modern basin waters (Hanor, 1994) suggests that the observed variations in fluid chemistry are not due to an approach to thermodynamic equilibrium with mineral assemblages in the source region. Thus, they more likely reflect processes occurring within the fluid aquifer on the flow path out of the basin or at the site of mineralization itself.

The apparent approach towards basin-buffered fluid compositions during evolution of the vein system can be explained in terms of mineral dissolution and precipitation reactions within the aquifer as fluids were expelled from the basinal source region, a process modeled and discussed by Sverjensky (1984). In this model, basinal fluids are initially in strong thermodynamic disequilibrium with the aquifer rocks resulting in extensive fluid-rock reactions, principally acid-neutralizing hydrogen metasomatism of silicates. This disequilibrium results in modification of fluid chemistry via dissolution-precipitation reactions. Gradually, as the buffer capacity of the mineral assemblages in the fluid conduit becomes exhausted, fluids within the aquifer approach the reservoir composition. Early neutralization of highly acidic (pH~4) basinal fluids would be capable of driving the fluid toward carbonate, anhydrite and/or barite saturation. In the present study, such a process could explain the initial precipitation of siderite in the vein system and the occurrence of anhydrite (fig. 4A). Precipitation of anhydrite, and locally barite, along the flow path could account for the lowering of Ca and Ba below typical basinal brine values. Similar variations in elements such as Sr are small in absolute terms; the high degree of correlation of Sr with Ca suggests that it substituted

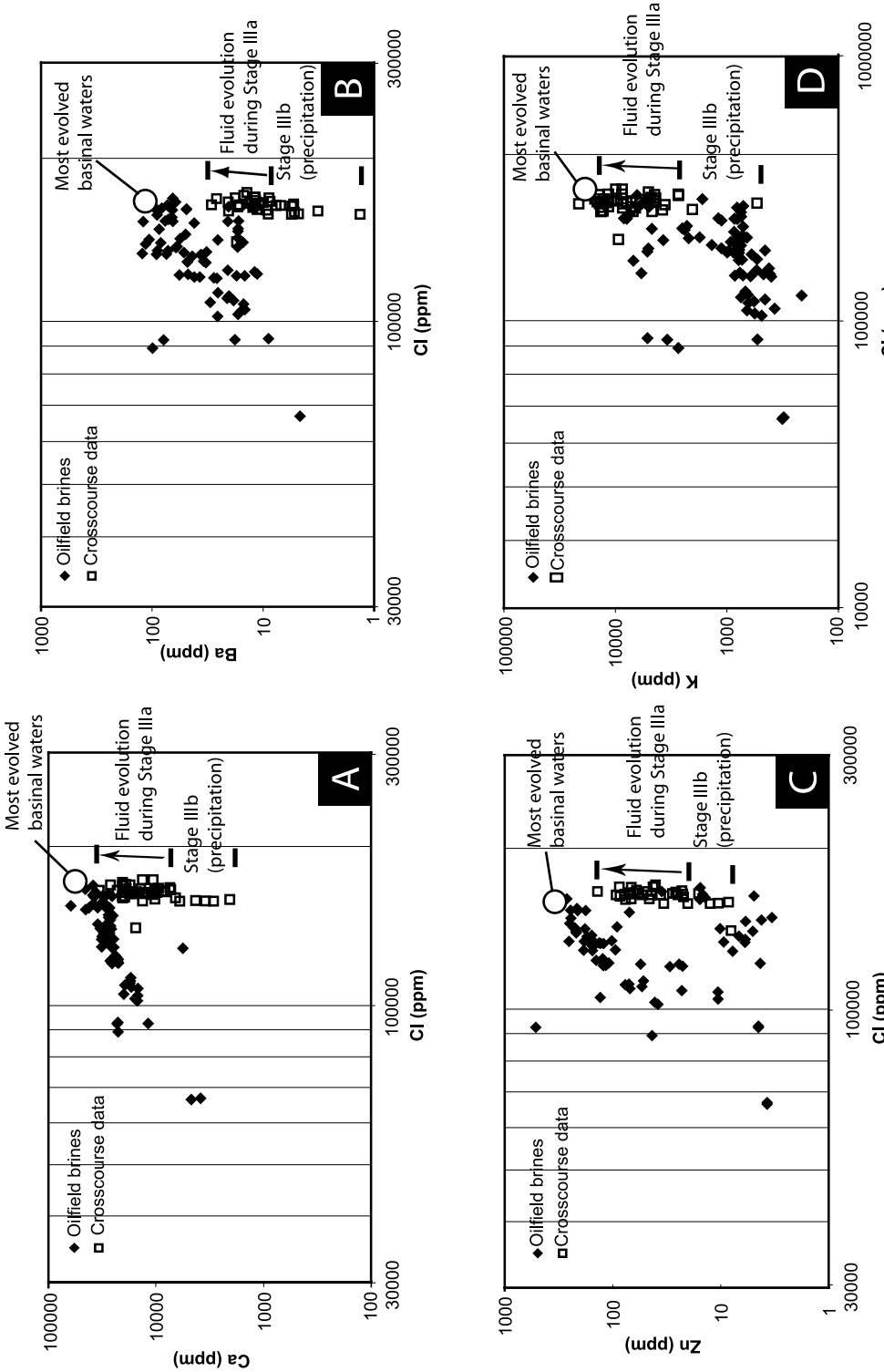

Fig. 10. Comparison of trends observed in Ca, Ba, Zn and K concentrations in the present study with typical modern oilfield brines. (Oilfield brine data from Carpenter and others, 1974), implying a possible evolution toward basin values.

as a trace constituent within precipitating calcic phases. The ubiquity of quartz within the veins during the latter stages of growth is consistent with the persistence of lower pH fluids further from the reservoir caused by the reduced buffering within the fluid conduit. Evidence for partial dissolution of previously formed sulfides could explain the observed increases in metals in Stage IIIa, perhaps as fluids became more acidic at a given point in the vein system through time. Buffering of the fluid close to galena and sphalerite saturation in the latter part of Stage IIIa is supported by the absolute values and small variation in the Zn:Pb ratio, which varies from 4.6 ± 2.5 to 1.7 ± 0.9.

The marked decrease in fluid salinity observed in Stage IIIb suggests that a significant fluid mixing (dilution) event occurred (fig. 8). However, dilution alone cannot account for the drop in element concentrations since all the element/Cl ratios also decrease significantly. We therefore consider the staggered reductions in Pb, Zn, Ba, Ca, Sr and K concentrations to be due to the sequential (and overlapping) precipitation of a number of minerals (galena, sphalerite, barite, anhydrite, muscovite) triggered by the fluid mixing event. Fine-grained anhydrite has been reported previously within growth zones in quartz from veins in the study area (fig. 4A, Gleeson, ms, 1997) as has K-mica (fig. 4B, Wilkinson, ms, 1990) and, although barite has not been observed locally, it is present in crosscourse veins elsewhere.

The existence of a second, dilute fluid in the study area at the time of mineralization has been documented previously, and local salinity variations in fluid inclusions from crosscourse vein samples in the area have been interpreted in terms of mixing between this fluid and the low temperature brine (Wilkinson, ms, 1990; Gleeson and others, 2000, 2001). The dilute fluid is thought to represent meteoric water that had extensively interacted with the Mylor Slate Formation by convective circulation in proximity to the Cornish granites at around 200°C (fig. 2). The data reported here suggest that the degree of dilution was limited, with less than 14 percent reduction in Cl concentrations recorded and no resolvable temperature increase. However, even this small degree of mixing appears to have been sufficient to promote significant mineral deposition, with in excess of 94 percent of the metal load and more than 85 percent of the Ca and Ba deposited. For the sulfides, this behavior is probably due to the fact that the solubility of base metals as chloride complexes is extremely sensitive to changes in chloride activity at a fixed temperature and $a.H_2S$ (Hanor, 1997). Precipitation of the sulfates could be controlled by a range of variables; however, the lack of information on the geochemistry of the dilute fluid precludes a more detailed analysis. Irrespective of the depositional mechanism, an apparent paradox is the lack of the abundant anhydrite that might be expected from such significant calcium loss. One explanation is that it could have been precipitated and then redissolved during subsequent stages of brine flow, perhaps associated with cooling of the system, analogous to the process known to occur in submarine hydrothermal vents (James and Elderfield, 1996). This interpretation is supported by the recent recognition of quartz pseudomorphs after anhydrite in the Porthleven crosscourse veins (Ickert and Gleeson, 2003).

Spatially, the main zone of decreased metal concentrations occurs just prior to the appearance of sulfides in the sample suggesting that, similar to Stage IIIa, the fluid inclusion assemblage is recording a precipitation event beyond the scale of the sample. A second, less significant, decrease recorded at analysis #36 to 37 coincides with a sudden drop in Cl and the appearance of galena in the sample and therefore may be directly linked to the local precipitation of sulfides driven by more extensive or proximal fluid mixing. The appearance of K-mica in growth zones in Stages IIIb to IV (Wilkinson, ms, 1990; see fig. 4) may account for the drops in K concentration through analyses #34 to 36 and #43 to 46.

Apart from a small drop in the K, Pb, Zn, Ba and Cl concentrations at analysis #44 that is likely to be caused by another minor mixing event, the data in Stage IV suggest that a return to a fairly stable brine infiltration of the vein system occurred. These fluids approximate the composition of evolved basinal waters similar to the fluids present in the latter part of Stage IIIa.

Control of Metal Ratios

Previous work on base-metal bearing basinal brines (Carpenter and others 1974; Hanor, 1994) has used the correlation between dissolved concentrations of Pb, Zn and Fe and stratigraphic interval to suggest that these metals were derived from reduction of iron oxide grain coatings in red bed units. If this were the case, then the putative source region for the mineralizing brines in this study, the basins of the Western Approaches Trough, would provide an excellent source of metals because the basin contains at least 6km of Carboniferous-Triassic red bed sequences (Evans, 1990; Gleeson and others, 2000). Another possible source for metal within the basin is the liberation of Pb from K-feldspar during alteration to sericite (Helgeson, 1967).

We suggest that the Permo-Triassic red bed source for the mineralizing brines examined in this study was favorable for the generation of relatively Pb-rich solutions as observed at the start of Stage III. The Pb-rich solutions resulted in the predominance of galena as a sulfide phase in the veins and in sphalerite only being precipitated once the excess Pb had been deposited. Mass balance considerations show that the total mass of Pb precipitated per kg of fluid in Stages IIIa and IIIb ($\sim$0.29g and $\sim$0.06g respectively) was greater than Zn ($\sim$0.06g and $\sim$0.07g respectively), consistent with the Pb-rich tenor of the veins. Selective precipitation does not appear to have played a significant role in controlling metal ratios in the deposit.

Concluding Remarks

There is no doubt that there is much to learn about the evolution of solution chemistry during formation of hydrothermal veins and that we have barely begun to resolve such variations let alone understand them. It is clear that the laser ablation technique has much to offer in this regard, although it will also be necessary to carry out numerical modeling based on well-constrained fluid chemistry to fully comprehend the complex chemical variability that is likely to be inherent in hydrothermal systems.

CONCLUSIONS

The ability to analyze the chemistry of individual, paragenetically-constrained fluid inclusions with good precision has enabled the resolution of a complex fluid evolution within a texturally simple, mineralized quartz vein. It is suggested that systematic and relatively long time-scale changes in brine chemistry are controlled by dissolution-precipitation reactions occurring within the fluid aquifer after fluid expulsion from the basin source region. Brines transporting up to 295 ppm Pb and 138 ppm Zn initially precipitated significant amounts of galena possibly due to reduction when they first encountered the carbonaceous and pyritic Mylor Slate Formation. Subsequently, a number of relatively short time-scale fluid mixing events led to further precipitation of galena with sphalerite and a number of other vein-forming phases. In the major precipitation events the depositional efficiency appears to have been very high, at over 94 percent for Zn and over 98 percent for Pb. Significantly, the fluid inclusion data appear to record precipitation events occurring beyond the scale of an individual hand sample, implying that fluid inclusions in hydrothermal veins can trap solutions depleted after transient mineral precipitation events upstream.

ACKNOWLEDGMENTS

We are grateful for the constructive comments on our original submission provided by Jacob Hanley, Paul Sylvester, Zachary Sharp and two anonymous referees. We also thank J. Spratt and T. Greenwood of the Natural History Museum, London for assistance with SEM analyses. This work was carried out during the MSci research project of BS, and was partly supported by the Department of Earth Science and Engineering, Imperial College London.

References

Alderton, D. H. M., 1978, Fluid inclusion data for lead-zinc ores from SW England: Transactions of the Institution of Mining and Metallurgy (Section B: Applied Earth Science), v. 87, p. 132–135.

Anderson, G. M., 1973, The hydrothermal transport and deposition of galena and sphalerite near 100°C: Economic Geology, v. 68, p. 480–492.

Barnes, R. P., and Andrews, J. R., 1981, Pumpellyite-actinolite grade regional metamorphism in South Cornwall: Proceedings of the Ussher Society, v. 5, p. 139–146.

Borisenko, A. S., 1977, Study of the salt composition of solutions in gas-liquid inclusions in minerals by the cryometric method: Soviet Geology and Geophysics, v. 18, p. 11–19.

Carpenter, A. B., Trout, M. L., and Pickett, E. E., 1974, Preliminary report on the origin and chemical evolution of lead- and zinc-rich oilfield brines in Central Mississippi: Economic Geology, v. 69, p. 1191–1206.

Chesley, J. T., Halliday, A. N., Snee, L. W., Mezger, K., Shepherd, T. J., and Scrivener, R. C., 1993, Thermochronology of the Cornubian batholith in southwest England: Implications for pluton emplacement and protracted hydrothermal mineralisation: Geochimica et Cosmochimica Acta, v. 57, p. 1817–1835.

Dines, H. G., 1956, The metalliferous mining region of southwest England: British Geological Survey Memoir, HMSO, London, 795 p.

Evans, C. D. R., 1990, United Kingdom offshore regional report: The geology of the western English Channel and its western approaches: British Geological Survey, HMSO, London, 93 p.

Ghazi, M. A., McCandless, T. E., Vanko, D. A., and Ruiz, J., 1996, New quantitative approach in trace elemental analysis of single fluid inclusions: applications of laser ablation inductively coupled plasma mass spectrometry (LA-ICP-MS): Journal of Analytical Atomic Spectrometry, v. 11, p. 667–674.

Gleeson, S. A., ms, 1997, The Geochemical Evolution of Mineralising Brines, South Cornwall, U. K.: Ph. D. Thesis, United Kingdom, Imperial College London, 317 p.

Gleeson, S. A., Wilkinson, J. J., Shaw, H. F., and Herrington, R. J., 2000, Post-magmatic hydrothermal circulation and the origin of base metal mineralisation, Cornwall, UK: Journal of the Geological Society, London, v. 157, p. 589–600.

Gleeson, S. A., Wilkinson, J. J., Stuart, F. M., and Banks, D. A., 2001, The origin and evolution of base metal mineralising brines and hydrothermal fluids, South Cornwall, UK: Geochimica et Cosmochimica Acta, v. 65, p. 2067–2079.

Günther, D., and Heinrich, C. A., 1999, Enhanced sensitivity in laser ablation-ICP mass spectrometry using helium-argon mixtures as aerosol carrier: Journal of Analytical Atomic Spectrometry, v. 14, p. 1363–1368.

Günther, D., Frischnecht, R., Heinrich, C. A., and Kahlert, H. J., 1997, Capabilities of an argon fluoride 193 nm Excimer laser for laser ablation inductively coupled plasma mass spectrometry microanalysis of geological materials: Journal of Analytical Atomic Spectrometry, v. 12, p. 939–944.

Günther, D., Audétat, A., Frischnecht, R., and Heinrich, C. A., 1998, Quantitative analysis of major, minor and trace elements in fluid inclusions using laser ablation-inductively coupled plasma mass spectrometry: Journal of Analytical Atomic Spectrometry, v. 13, p. 263–270.

Hanor, J. S., 1994, Origin of saline fluids in sedimentary basins, *in* Parnell, J., editor, Geofluids: Origin, Migration and Evolution of Fluids in Sedimentary Basins: Geological Society of London Special Publications, v. 78, p. 151–174.

——— 1997, Controls on the solubilization of dissolved lead and zinc in basinal brines, *in* Sangster, D.F., editor, Carbonate-hosted lead-zinc deposits: Society of Economic Geologists Special Publication 4, p. 483–500.

Heinrich, C. A., Pettke, T., Halter, W. E., Aigner-Torres, M., Audetat, A., Gunther, D., Hattendorf, B., Bleiner, D., Guillong, M., and Horn, I., 2003, Quantitative multi-element analysis of minerals, fluid and melt inclusions by laser-ablation inductively-coupled-plasma mass-spectrometry: Geochimica et Cosmochimica Acta, v. 67, p. 3473–3496.

Helgeson, H. C., 1967, Silicate metamorphism in sediments and the genesis of hydrothermal ore solutions, *in* Brown, J. S., editor, Genesis of stratiform lead-zinc-barite-fluorite deposits: Economic Geology Monograph 3, p. 333–342

Huston, D. L., and Large, R. R., 1987, Genetic and exploration significance of the zinc ratio (100 Zn/(Zn+Pb)) in massive sulfide systems: Economic Geology, v. 82, p. 1521–1539.

Ickert, R., and Gleeson, S. A., 2003, Cathodoluminescence zonation in hydrothermal vein quartz linked to enrichment in aluminium: Geological Society of America, Abstracts with Programs, v. 35, n. 6, p. 268.

Jackson, N. J., Willis-Richards, J., Manning, D. A. C., and Sams, M. S., 1989, Evolution of the Cornubian ore field, Southwest England: Part II. Mineral deposits and ore-forming processes: Economic Geology, v. 84, p. 1101–1133.

James, R. H., and Elderfield, H., 1996, Chemistry of ore-forming fluids and mineral formation rates in an active hydrothermal sulfide deposit on the Mid-Atlantic Ridge: Geology, v. 24, p. 1147–1150.

Jeffries, T. E., Jackson, S. E., and Longerich, H. P., 1998, Frequency quintupled (213nm) laser ablation microprobe inductively coupled plasma mass spectrometry: Journal of Analytical Atomic Spectroscopy, v. 13, p. 935–940.

McCandless, T. E., Lajack, D. J., Ruiz, J., and Ghazi, M. A., 1997, Trace element determination of single fluid inclusions in quartz by laser ablation ICP-MS: Geostandards Newsletter, v. 21, p. 279–287.

Oakes, C. S., Bodnar, R. J., and Simpson, J. M., 1990, The system NaCl-$CaCl_2$-H_2O: I. The ice liquidus at 1 atm. total pressure: Geochimica et Cosmochimica Acta, v. 54, p. 603–610.

Roedder, E., 1967, Environment of deposition of stratiform (Mississippi Valley-type) ore deposits, from studies of fluid inclusions: Society of Economic Geologists, Monograph 3, p. 349–362.

——— 1976, Fluid inclusion evidence on the genesis of ores in sedimentary and volcanic rocks, *in* Wolf, K.H., editor, Handbook of strata-bound and stratiform ore deposits; I. Principles and general studies; Vol. 2, Geochemical studies: New York, Elsevier, p. 67–110.

——— 1984, Fluid Inclusions: Reviews in Mineralogy, V. 12, Mineralogical Society of America, 646 p.

Scrivener, R. C., Darbyshire, D. P. F., and Shepherd, T. J., 1994, Timing and significance of crosscourse mineralisation in SW England: London, Journal of the Geological Society, v. 150, p. 587–590.

Shepherd, T. J., and Scrivener, R. C., 1987, The role of basinal brines in the genesis of polymetallic vein deposits Kit Hill-Gunnislake district, S.W. England: Proceedings of the Ussher Society, v. 6, p. 491–497.

Shepherd, T. J., Rankin, A. H., and Alderton, D. H. M., 1985, A practical guide to fluid inclusion studies: London, Blackie and Son, 239 p.

Skinner, B. J., 1997, Hydrothermal Mineral Deposits: What we do and don't know, *in* Barnes, H. L., editor, Geochemistry of Hydrothermal Ore Deposits, Third edition: New York, John Wiley and Sons, p. 1–29.

Sverjensky, D. A., 1981, The origin of a Mississippi Valley-Type deposit in the Viburnum Trend, Southeast Missouri: Economic Geology, v. 76, p. 1848–1872.

——— 1984, Oil field brines as ore-forming solutions: Economic Geology, v. 79, p. 23–37.

Wilkinson, J. J., ms, 1990, The origin and evolution of Hercynian crustal fluids, South Cornwall, England: Ph. D. Thesis, United Kingdom, University of Southampton, 298 p.

——— 2001, Fluid inclusions in hydrothermal ore deposits: Lithos, v. 55, p. 229–272.

Wilkinson, J. J., Jenkin, G. R. T., Fallick, A. E., and Foster, R. P., 1995, Oxygen and hydrogen isotopic evolution of Variscan crustal fluids, south Cornwall, U.K: Chemical Geology, v. 123, p. 239–254.

Willis-Richards, J., and Jackson, N. J., 1989, Evolution of the Cornubian ore field, Southwest England: Part I. Batholith modeling and ore distribution: Economic Geology, v. 84, p. 1078–1100.